Macromolecular Bioscience
www.mbs-journal.de

Stiffening by Osmotic Swelling Constraint in Cartilage-Like Cell Culture Scaffolds

*Giovanni S. Offeddu, Constantin E. Tanase, Sotiria Toumpaniari, Michelle L. Oyen, and Ruth E. Cameron**

Cartilage wounds result in chronic pain and degradation of the quality of life for millions of people. A synthetic cellular scaffold able to heal the damage by substituting the natural tissue is of great potential value. Here, it is shown for the first time that the unique interplay between the molecular components of cartilage can be reproduced in composite materials made of a polyelectrolyte hydrogel embedding a collagen scaffold. These composites possess a mechanical response determined by osmotic and electrostatic effects, comparable to articular cartilage in terms of elastic modulus, time-dependent response, and permeability to interstitial fluid flow. Made entirely from biocompatible materials, the cartilage-like composite materials developed permit 3D culture of chondrocyte-like cells through their microporosity. The biomimetic materials presented here constitute an entirely new class of osmotically stiffened composites, which may find use outside of biomedical applications.

1. Introduction

Articular cartilage, the smooth lining of long bones at the joint interface, degrades in people suffering from musculoskeletal conditions like osteoarthritis or those deriving from wear and tear of the tissue due to trauma.[1] Wounds in the cartilage layer expose the underlying bone, causing chronic pain and loss of mobility, thus degrading the quality of life for millions of people who are forced to give up an active lifestyle. Because cartilage is avascular and, therefore, very limited in its self-repair, treatment involves the partial or total replacement of the tissue.[1,2] Despite large research efforts directed at the creation of synthetic cellular scaffolds for the repair of articular cartilage, clinical solutions able to restore the original mobility of the joint remain elusive.[3,4]

Tissue engineering scaffolds must guarantee the viability of patient-specific cells while the synthetic construct is integrated as part of the native tissue. The scaffolds have also been shown to provide the cells seeded with tissue-conducive physical cues, in the form of substrate stiffness,[5–7] time-dependent relaxation,[8,9] as well as shear stresses arising from the movement of the interstitial fluid.[10] Scaffolds that can effectively reproduce the physical response of natural cartilage can, therefore, provide the cells seeded with physiological mechanical stimuli; at the same time, the mechanical properties of these scaffolds at the macroscale would guarantee the load-bearing capacity and quality necessary for the correct functioning of the joint. For these reasons, the investigation of new synthetic cellular environments for the repair of cartilage has been pursuing increasing levels of biomimesis, from the ionic make-up of single polymer chains at the nanoscale to the reproduction of the microscale compositional variation of the tissue with depth.[11,12]

The unique physical response of cartilage is yet to be reproduced in a synthetic material. The extra-cellular matrix (ECM) of articular cartilage is particular in that it can be fundamentally considered as a composite material, whereby collagen fibrils are embedded in a proteoglycan gel matrix.[13] However, unlike traditional composite materials, the matrix in cartilage does not only play a passive role; the large fixed charge density present on the proteoglycan glycosaminoglycan (GAG) chains produce an imbalance in the counter-ion concentration between the tissue and the external environment of the joint, giving rise to an osmotic swelling pressure.[14] This swelling is resisted by the collagen network, resulting in a pressurized system with unique, fit-for-purpose physical properties superior to those of the two components alone.

Inspired by the osmotically stiffened structure of cartilage, we present here a novel class of composite materials that make use of ionic effects to achieve a physical response comparable to that of cartilage. These materials are produced using biocompatible polymers and methods, hence allowing the investigation of their use for 3D cell culture.

Dr. G. S. Offeddu, Dr. C. E. Tanase, Dr. S. Toumpaniari, Prof. R. E. Cameron
Cambridge Centre for Medical Materials
Department of Materials Science and Metallurgy
University of Cambridge
27 Charles Babbage Rd, Cambridge CB3 0FS, UK
E-mail: rec11@cam.ac.uk
Dr. G. S. Offeddu, Dr. M. L. Oyen
The Nanoscience Centre
Department of Engineering
University of Cambridge
11 JJ Thomson Ave, Cambridge CB3 0FF, UK

DOI: 10.1002/mabi.201800247

2. Fabrication and Activation of Cartilage-Mimetic Composite Materials

The properties of the proteoglycan gel matrix found in cartilage can be reproduced using polyelectrolyte hydrogels. These materials present fixed negative charges reminiscent of those found on the GAGs of cartilage, and have recently attracted attention as cellular scaffolds for the repair of this and other electroactive tissues like bone and muscle.[15,16] Blends of poly(vinyl alcohol) (PVA) and poly(acrylic acid) (PAA) can be cross-linked by repeated freeze-thawing cycles, yielding microporous cryogels where PVA acts as the mechanically stable cross-linked backbone, while PAA possesses negative charges that are active at physiological pH and ionic strength.[11,17] An increasing number of freeze-thaw cycles results in a larger amount of both polymers fixed in the cross-linked network, therefore in a larger fixed charge density. Introduction of such polyelectrolyte cryogels within a porous reinforcing material can be used to reproduce the interpenetrating network found in natural cartilage.

The PVA–PAA polymer blend is cross-linked inside type I collagen freeze-dried scaffolds (**Figure 1**a). These microporous materials, which were used in Yannas and coworkers' pioneering research on skin regeneration,[18] have since then been used in multiple clinical studies targeting the repair of other tissues and whole organs,[19] as well as to study the in vitro behavior of several cell types.[20–22] Their exceptional biocompatibility and biodegradability make them ideal platforms for composite materials mimicking natural ECMs. The composites here fabricated with polyelectrolyte cryogels are initially in a neutral state, as the pH of the polymer solution during fabrication is below the pKa of PAA (≈4.5).[23] Activation of the fixed negative charges is carried out by increasing the pH to 13 in order to fully ionize PAA, followed by stabilization in cell culture media to simulate physiological pH and ionic strength.

The presence of fixed charges on the solid hydrogel network has a different effect on the composite materials and the cryogel components alone. Figure 1b,c shows that activation resulted in swelling of both types of materials, as the polyelectrolytes imbibed more water to balance the counter-ion concentration differential. In particular, the swelling of the cryogel component is reduced with increasing numbers of freeze-thaw cycles, c. The phenomenon was previously explained as due to the increasing elastic resistance to swelling that the larger amount of polymer offers,[17] with the measured values of volumetric swelling ratio Q_V comparable to those at pH 13 previously reported.[11] In the composite materials, the presence of the collagen scaffold surrounding the polyelectrolyte cryogels results in significant less swelling than the cryogel component alone. In addition, the swelling is observed to be constant with c (average = 1.76, $p > 0.05$) and comparable to that reported for the collagen component alone.[24]

In articular cartilage, the collagen network restrains the size of the proteoglycans matrix to one fifth of their fully swollen volume.[13] The extent of this restraining action is comparable

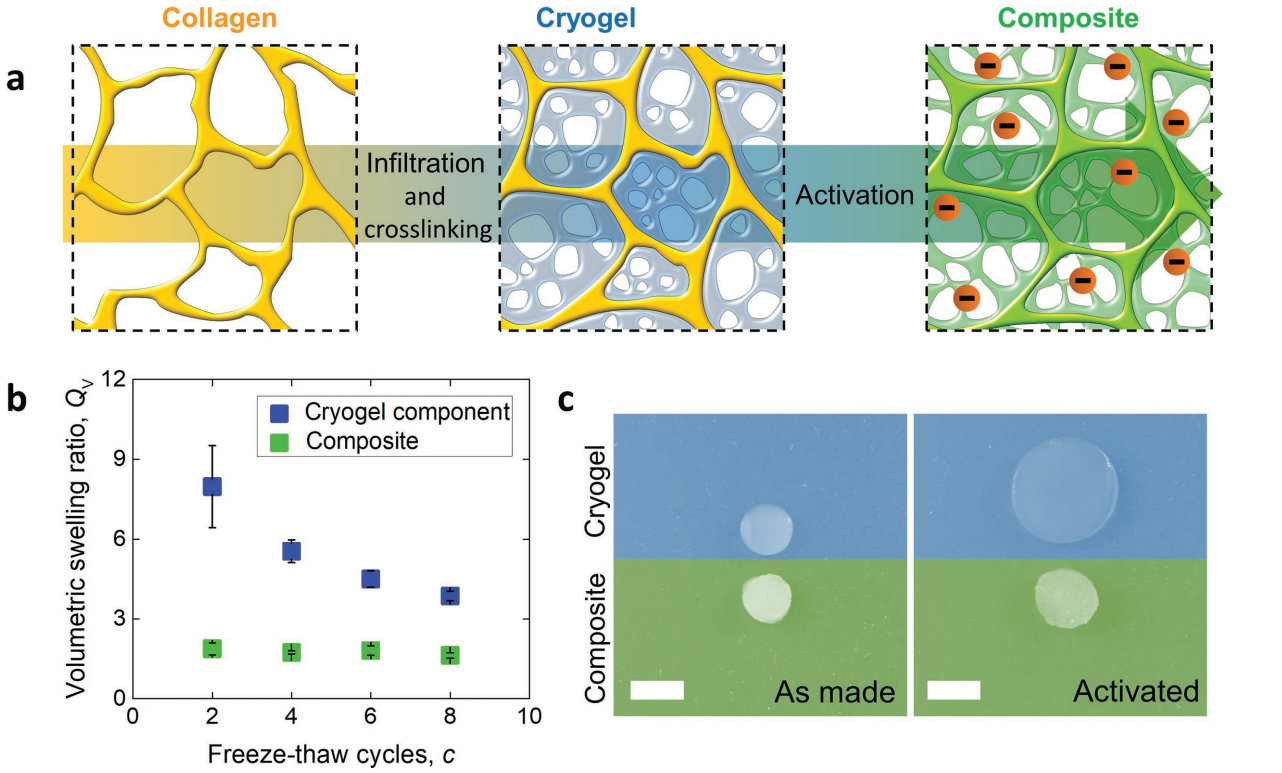

Figure 1. Collagen scaffolds constrain swelling of polyelectrolyte cryogels. a) Schematic of composite preparation: a freeze-dried collagen scaffold is infiltrated with a solution of PVA and PAA, then cross-linked by freeze-thawing. The composite produced is subsequently activated at large pH. b) Swelling of the composites upon activation as compared to that of the cryogel components, which always swell to greater extents. Error bars indicate the standard deviation, $n = 4$. c) Comparison between photographs of a composite and its cryogel component after two freeze-thaw cycles. The scale bar is 5 mm.

to that observed for the composites presented here after two freeze-thaw cycles, and is of the same order of magnitude even for larger values of c, as the overall swelling is ultimately determined by that of the collagen component alone. We anticipated that the constraint imposed on the charged hydrogel within the collagen scaffold would affect the mechanical properties of the composite materials.

3. Osmotic Constraint Produces Cartilage-Like Physical Properties

The composite materials presented here reproduce the interplay found in natural cartilage between the charged polyelectrolyte matrix and the restraining collagen network. While the ECM of cartilage possesses nanoscale morphological features,[13] the materials used as part of this study possess an inherent microporosity necessary for the seeding of cells. Nevertheless, in both cases, the constraint of the charged matrix results in an imbalance in positive counter-ions between the material and the environmental solution (**Figure 2**a). This imbalance gives rise to an osmotic swelling pressure (Figure 2b) that, when imposed on the collagen network, produces mechanical effects that have so far been unique to cartilage.

The time-dependent mechanical response of the materials investigated was measured by spherical indentation, a technique commonly used to study the compressive properties of cartilage.[25,26] An initial indentation ramp in displacement is followed by a hold at constant indentation depth, over which the load measured decreases to an equilibrium value. Analysis of this load relaxation profile can yield much information regarding the time-dependent response of the samples. Figure 2c shows the effect of fixed charges activation on the compressive elastic modulus E of the composites. These materials possess an elastic modulus of approximately 100 kPa in the neutral state (average 116.4 kPa, $p > 0.05$). Upon activation, however, the elastic modulus increases by one order of magnitude to approximately 1 MPa (average 947.9 kPa, $p > 0.05$). This value is not only strikingly larger than that in the neutral state, but it also falls within the range expected for articular cartilage (0.36–1.11 MPa).[27]

The elastic modulus of constrained polyelectrolyte hydrogels can be predicted from the swelling pressure, ω, that these materials exert. The swelling pressure results from three contributions.[28]

$$\omega = \pi_{mix} + \pi_{el} + \pi_{ion} \quad (1)$$

where π_{mix} is the contribution due to the polymer–solvent mixing, π_{el} to the elasticity of the polymer network resisting the swelling, and π_{ion} to the nonuniform distribution of counterions, that is, the contribution dependent on the fixed charge density and increasing with this parameter. The explicit form of each contribution is provided as part of the Supporting Information, together with the swelling pressure and fixed charge density ranges for the composite materials presented here and for natural cartilage (Figure S1, Supporting Information). The osmotic modulus contribution, E_{OSM}, is given by[29]

$$E_{OSM} = 3(1-2\nu)\varphi_p(d\pi/d\varphi_p) \quad (2)$$

where ϕ_p is the polymer (PVA and PAA) volume fraction and the Poisson's ratio ν can be taken as 0.33 for microporous materials.[30] The effect of the collagen constraint can be included in this analysis by considering the polyelectrolyte hydrogel contained within each collagen scaffold pore to be constrained in 3D by all other pores surrounding it,[31] so that

$$E = E_{OSM}(1-\nu)/(1-\nu-2\nu^2) \quad (3)$$

Based on the analysis above, the predicted elastic modulus of the activated composites is shown in Figure 2c together with the measured values. The prediction was successful ($p > 0.05$), yet the expected small increase in modulus as a result of increasing fixed charge density with c was hidden by the variability in the measurements.

The movement of pressurized fluid away from the area of indentation over time contributes to the load relaxation of hydrated soft materials and tissues.[26] The ease with which the interstitial fluid can move through a porous solid is determined by the hydraulic permeability K of the particular morphology. This parameter also affects the cells present within the structure, as the shear stresses imposed by the fluid flow increase with decreasing permeability.[32] Cartilage has a relatively small hydraulic permeability (10^{-16} to 10^{-15} $m^4(N\ s)^{-1}$),[33] necessary to avoid excessive fluid loss from the tissue upon movement. As reported in Figure 2d, the permeability of the composite materials here developed decreases upon activation of the fixed charges, a phenomenon previously observed for the polyelectrolyte cryogel component and even natural cartilage,[11,34] and explained as due to an increased electrostatic interaction between the charged polymer network and the fluid. The permeability achieved by the activated composites is within the range expected for cartilage (average 5.82×10^{-15} $m^4(N\ s)^{-1}$, $p > 0.05$).

The overall load relaxation of hydrated soft materials is produced by both fluid flow-dependent effects and viscoelastic relaxation of the polymer. The extent of this load relaxation can be quantified by the viscoelastic ratio R, which varies between 1 for a purely elastic response (no relaxation) and 0 for a purely viscous response (complete relaxation).[35] Articular cartilage is known to relax to a great extent, possessing a value of R reportedly between 0.11 and 0.22.[35,36] The activated biomimetic composites again possess properties comparable to those of natural cartilage, with the value of R lying very close to the range expected for cartilage (average 0.25 and $p > 0.05$ when excluding the measurement after two freeze-thaw cycles). In the neutral state, the composites are more elastic, with the difference between states possibly due to different interfacial effects between the two components.

4. Mechanical Comparison with Single Components

Introduction of a polyelectrolyte hydrogel within the collagen scaffold results in dramatic changes in mechanical properties. Strikingly, these changes are reliably constant regardless of number of freeze-thaw cycles imposed on the cryogel

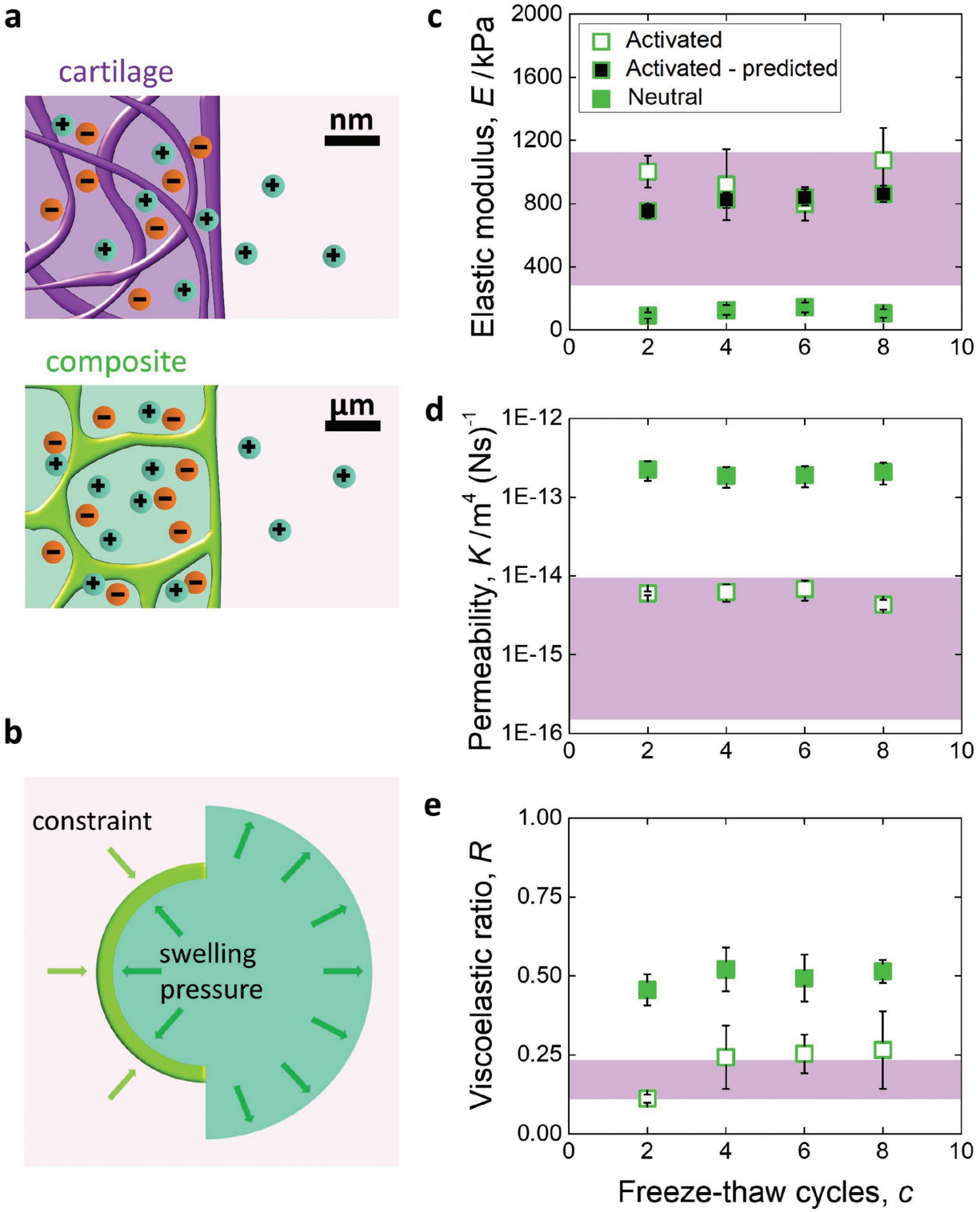

Figure 2. Osmotic composites possess cartilage-like mechanical behavior. a) Ionic environment found in natural cartilage and reproduced in the composite materials. The concentration of positive counter-ions is larger compared to the environmental solution due to the presence of negative fixed charges. b) Osmotic swelling pressure generated by the ionic imbalance. c–e) Mechanical response of the composites as a function of activation state, where the indentation elastic modulus (c) increases, and the permeability to fluid flow (d) and viscoelastic ratio (e) decrease with the activation of the fixed charges. The shaded area represents the range of values expected for natural cartilage, as reported in-text. In (c), the predicted elastic modulus of the activated composites as a result of fixed charge density and constrain by the collagen is also reported. Error bars represent the standard deviation, $n = 4$.

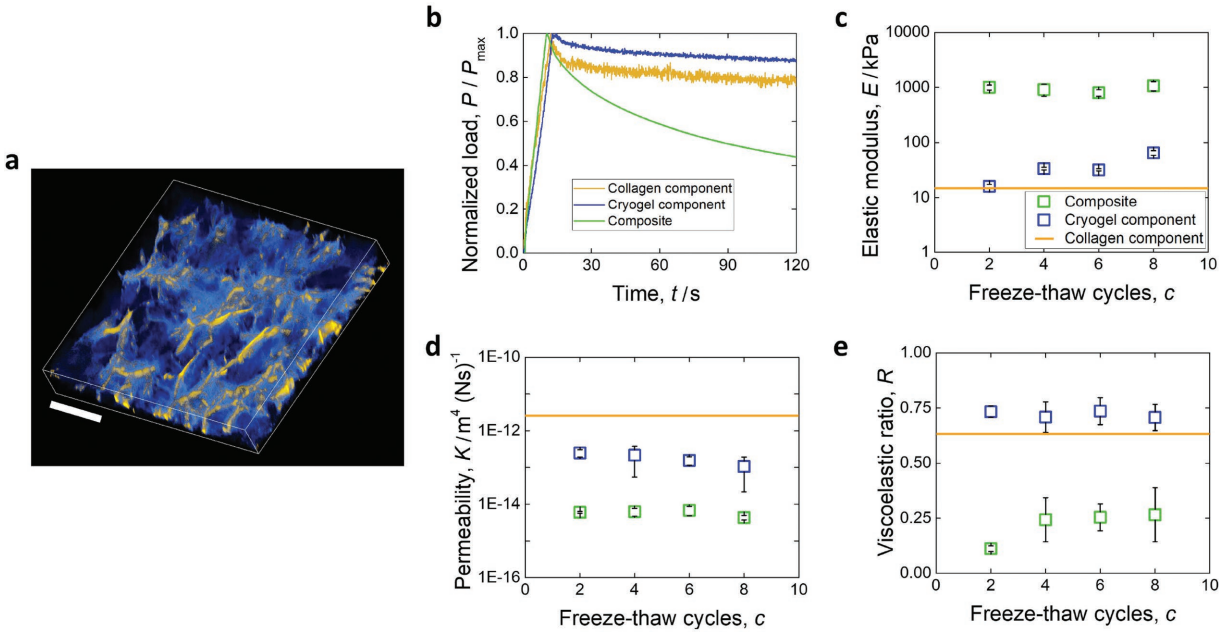

Figure 3. Mechanical response of composites is not comparable to that of the single components. a) 3D confocal microscopy projection (800 × 800 × 100 μm) of a composite showing the microporous characteristic of the two single components through the depth. The scale bar is 200 μm. b) Time-dependent load relaxation of the composites and single components. The load is normalized to the maximum load achieved to compare the relaxation for the different materials. c–e) Mechanical response of activated composite scaffolds as compared to that of their collagen and cryogel components, when subjected to similar environmental conditions. The elastic modulus (c) is one to two orders of magnitude larger for the composites, while their permeability to fluid flow (d) is two to three orders of magnitude smaller. The viscoelastic ratio (e) is also significantly smaller for the composites compared to the single components. Error bars represent the standard deviation, $n = 4$.

component, that is, its fixed charge density. This result suggests that, similarly to the swelling extent measured upon activation, the properties of the composites are principally determined by the collagen scaffold and its restraining action. Yet, such properties are very different from those of the single collagen and cryogel components.

Figure 3a shows that the two components can be discerned within the composites and they retain their characteristic microporous morphology. However, the activated composites possess a mechanical response with time significantly different from the two components (Figure 3b). The elastic modulus of the activated composites is one-to-two orders of magnitude larger than the single components when these are subjected to the same activation procedure (Figure 3c), due to the osmotic-stiffening taking place when the activation-independent collagen restrains the swelling of the polyelectrolyte cryogels. The hydraulic permeability is instead much larger for the single components (Figure 3d), most likely due to the smaller solid fraction and, therefore, increased fluid flow path's size. Both components behave more elastically than the composites (Figure 3e), again suggesting that interfacial phenomena between the two components give rise to large amounts of viscoelastic relaxation in the composites.

The mechanical characterization of the single components reveals broad differences between their mechanical behavior and that of the composites. As these materials may be used for the culture of chondrocytes aimed at the repair of cartilage, the question arose as to whether the different physical cues they present would affect the biological activity of cells seeded within.

5. 3D Cell Culture in the Composite Microenvironment

Human chondrocyte-like cells (SW1353 chondrosarcoma cell line) were seeded on the composite materials and single components alike. For both the composites (C) and the cryogel (G) components, the materials were assessed after two (2FT) and eight (8FT) freeze-thaw cycles. First, the seeding efficiency S_{eff} (**Figure 4**a), which represents the percentage of cells adhered on the materials after seeding, was measured by counting the fraction of cells present on the materials following incubation for 3 h. The collagen component shows the largest average number of adherent cells ($p < 0.05$ compared to all other conditions), most likely due to the large number of specific cell-binding sites this material presents.[37] The cryogel components show the smallest average cell seeding efficiency, possibly because the PVA making up most of the structure has poor cell-adhesion properties,[38] while the composites show values in between those of the two single components. No difference is observed between the materials resulting from two or eight freeze-thawing cycles.

The ability of cells to reach large depths within synthetic scaffolds is of paramount importance to ensure homogeneity of the tissue formed, particularly in the case of cartilage where vasculature is not present to aid cell mobility.[27] Analysis of cell position, l, by day 14 reveals that the mean cell depth is largest in the collagen scaffolds (Figure 4b, $p < 0.05$), while no significant difference can be observed between the other conditions. In all materials, cells are observed at a depth approaching 1 mm by

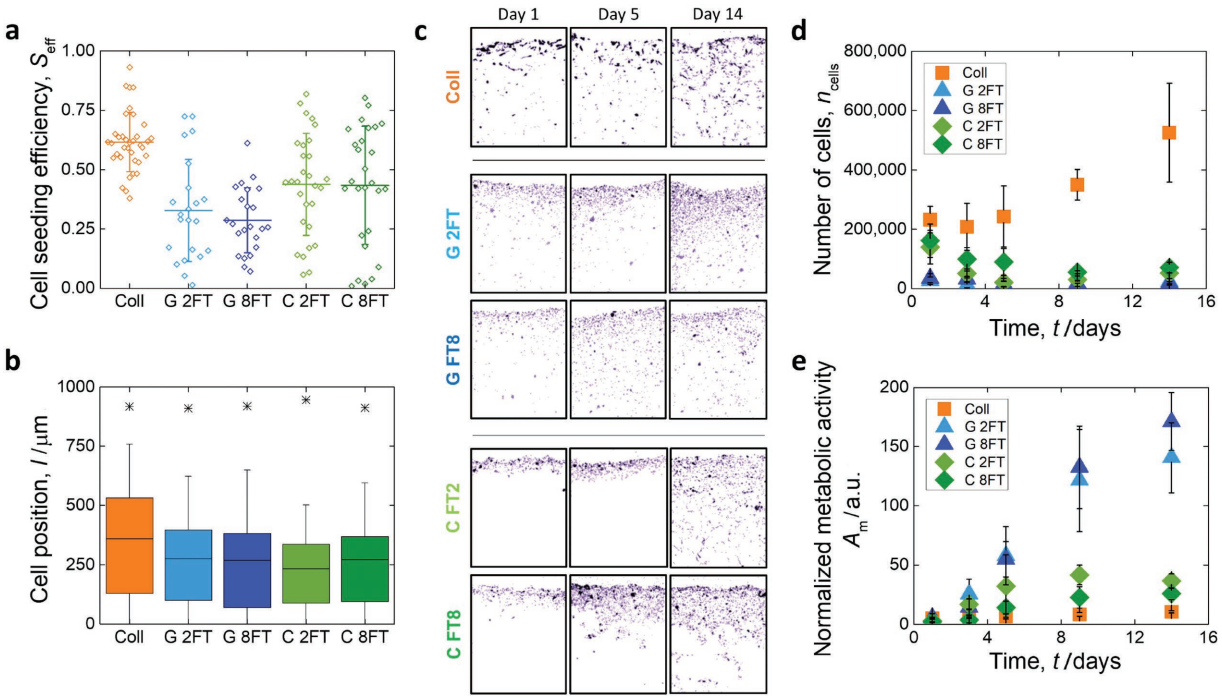

Figure 4. Chondrocyte-like cells adhere to, migrate through, and remain viable within the composites and single components. a) Cell seeding efficiency for the collagen (Coll) and cryogel components (G) and their composite materials (C), where the average number of cells adhered to the composites is in between those of the components. b) Cell depth after 14 days of tissue culture. The mean position is shown (horizontal line), together with the standard deviation (whiskers) and the maximum depth observed (asterisks). c) Confocal microscopy projections of the cells as a result of material and time. Each micrograph is 800 × 1000 µm. d) Number of cells within the different materials as a function of time. Cells remain viable in all materials and proliferate within the collagen scaffolds. e) Metabolic activity of single cells within the 3D composites and single components, as a function of tissue culture time.

day 14. The confocal microscopy images shown in Figure 4c depict chondrocyte positions at different times after seeding. On day 1, cells are observed at greater depths within the collagen and cryogels compared to the composites. Through day 14, the maximum cell depth remains constant for the single components (Figure S2, Supporting Information), suggesting that the larger porosity of these structures facilitates the infiltration on day 1. In the composites, the average and maximum cell depths instead increase with time ($p < 0.05$), implying that cells are able to migrate through these materials.

The number of cells present on the materials changed differently with time (Figure 4d). Proliferation was observed in the collagen scaffolds over 14 days ($p < 0.05$), while in the cryogels the number of cells did not change over the same time period ($p > 0.05$). In the composite materials, the number of cells on day 1 is in between the collagen and cryogel components, as expected from the cell seeding efficiency results. However, before day 3, the cell number falls, to then remain constant up to day 14, both for materials after two and eight freeze-thaw cycles ($p > 0.05$). As more of the cells in the composites were positioned on the surface and, therefore, more exposed to the external culture environment, a fraction likely detached after day 1. The stable cell number observed in both composites and cryogels could be due to equilibrium between adherent proliferative and de-adhering cells, or lack of proliferation as they become quiescent chondrogenic cells.[39] In fact, it is possible that the increased osmolarity in those materials, varying linearly with the fixed charge density (Figure S1, Supporting Information), may have altered the functionality of the chondrocyte-like cells seeded within.[40]

Chondrocytes in mature cartilage present a round morphology, low metabolic activity, and lack of proliferation.[41] Analysis of the metabolic activity of cells within the different 3D environments shows that the chondrocytes are consistently more active in the cryogel components than the collagen component, possibly the result of difficulties in maintaining attachment,[42] while the metabolic activity in the composites is in between the two and closer to the low levels within the collagen environment (Figure 4e). For all materials, the metabolic activity of single cells increases over time ($p < 0.05$).

To better visualize and understand the interaction between the cells and the materials making up the composites, 2D films were fabricated using collagen or PVA–PAA hydrogels, cross-linked in the same fashion and to the same extent as in the 3D scaffolds. The cell morphology was investigated over 5 days, during which cells on the collagen retain their characteristic fibroblast-like shape, where the actin filaments are prominent (**Figure 5**a) indicating strong cell adhesion on the substrate.[43] The cells on the cryogel substrates have a round shape (Figure 5a–c) with visible actin monomers and, in some cases, blebbing, both signs of poor adhesion to the substrate.[44] The cell population on the collagen substrates increases over time ($p < 0.05$), similarly to the 3D collagen component case.

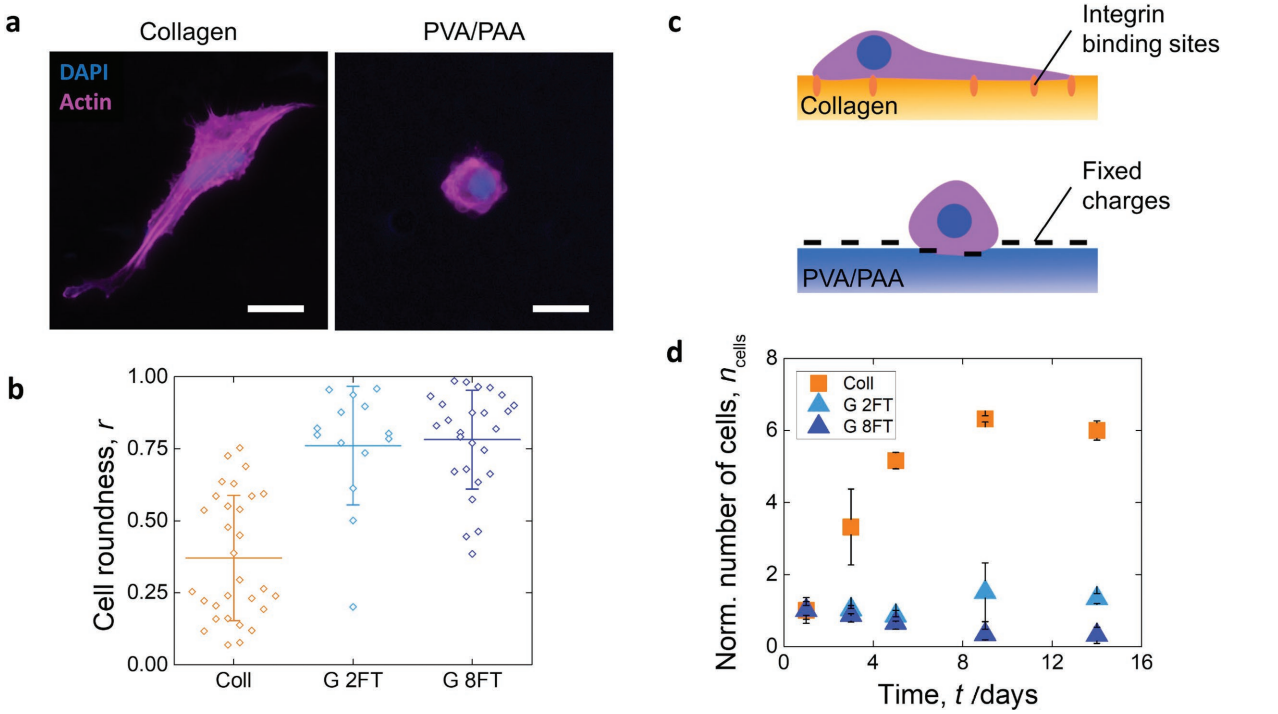

Figure 5. Interaction between cells and composite components determines cell morphology and activity. a) Cell-materials interaction was investigated by fluorescence microscopy of cells seeded on the top of 2D components. The images shown are from cells cultured for 5 days, and representative of the entire time of the study conducted. The scale bar is 20 µm. b) The cell roundness is reported as a ratio varying between 1 (circular shape) and 0 (linear shape). c) Schematic diagram of cell-substrate interaction and resulting morphology. d) Normalized number of cells (compared to day 1) present on the 2D components over 14 days of culture. Error bars represent the standard deviation, $n = 6$.

Instead, the number of cells on the PVA–PAA substrates remains stable (2FT, $p > 0.05$), or even decreases (8FT, $p < 0.05$) during the 14 day culture (Figure 5d), likely because some of the cells detach due to poor attachment to the substrate. The viability results in 3D are in accordance with the results from the 2D studies suggesting that cell–matrix interactions play a major role in the viability and behavior of the cells.

Overall, these results show that the composite materials developed can be used to culture cells in 3D and provide interesting cartilage-like cues to the chondrocytes seeded. The presence of the collagen component provides specific binding sites for cell attachment, resulting in low cell metabolic activity. At the same time, the charged cryogel component in the composites results in arrested proliferation of the cells, as well as in a cell morphology closer to that expected in vivo.

6. Conclusion

The composite materials presented here reproduce for the first time the unique interplay between the ECM components of articular cartilage. The osmotic, electrostatic, and interfacial phenomena between polyelectrolyte hydrogels and the collagen scaffold embedded within result in a mechanical behavior comparable to that of natural cartilage. Made entirely from biocompatible polymer, these biomimetic composites allow the successful 3D culture of chondrocyte-like cells. Further studies involving entirely biodegradable materials will be necessary to apply the methodology developed herein to scaffolds that may be translated to the clinic. The mechanical response achieved by the composites created, indeed, can be reproduced in other materials systems that couple a polyelectrolyte hydrogel with a reinforcing component able to constrain its swelling. These osmotically stiffened materials can find applications outside the biomedical field, from actuation to sensing, and represent an entirely new class of composite materials.

7. Experimental Section

Fabrication and Activation of Composite Materials: Insoluble fibrillar type I collagen from bovine Achilles tendon (Sigma Aldrich, UK) was used for the fabrication of the collagen scaffold component as previously described.[24] Briefly, collagen was suspended in acetic acid (1% w/v in 0.05 M, Alfa-Aesar, UK) and subsequently blended and centrifuged at 2500 rpm for 15 min to remove any air bubbles. The homogeneous slurry produced was frozen in a VirTis adVantage bench-top freeze-drier (Biopharma Process Systems, UK) at –20 °C for 2 h, following a cooling rate of 0.5 °C min^{-1} from room temperature. Drying at 0 °C was carried out under a vacuum of 80 mTorr for 20 h. The scaffolds produced were cross-linked using 1-ethyl-3-(3-dimethylaminopropyl) carbodiimide hydrochloride (EDC, Sigma Aldrich, UK) and N-hydroxysuccinimide (NHS, Sigma Aldrich, UK), dissolved in 95% v/v ethanol in water in a molar ratio 5:2:1 relative to the collagen carboxyl groups (EDC: NHS: COOH). After washing in water for 15 min, the scaffolds were freeze-dried once again using the process described above.

The collagen scaffolds were infiltrated with a solution of PVA (average molecular weight 33 000 g mol^{-1}, Sigma Aldrich, UK) and PAA (average

molecular weight 140 000 g mol^{-1}, Sigma Aldrich, UK), both used without further purification. The polymers were separately dissolved in water at 85 °C over 8 h at a concentration of 15% w/w, after which the two solutions were mixed in a mass ratio of 3: 1, PVA:PAA. Infiltration was carried out on a shaker plate held at 37 °C for 48 h. The samples were de-gassed to facilitate infiltration after 24 h for 30 min with a vacuum of 1200 mTorr. The PVA–PAA blend solution within the collagen scaffold was cross-linked into a cryogel by freeze-thawing, as previously described[11]: Freezing of the infiltrated scaffolds at −20 °C for 8 h was followed by thawing at room temperature for 4 h. The freeze-thaw cycle was repeated between two and eight times.

Activation of the composite materials produced was achieved by, first, immersion in a 0.1 M NaOH solution (Sigma Aldrich, UK) overnight, followed by washing in complete cell culture medium (as detailed below) for over 4 h. The volumetric swelling ratio Q_V of the composites was calculated as

$$Q_V = (D_a / D_n)^3 \quad (4)$$

where D_a and D_n are the lateral sizes of the samples in the activated and neutral (as-made) states, respectively, assuming isotropic swelling. In the analysis, swelling is intended as the bulk swelling of the materials due to additional fluid filling of the microscopic pores in the structures, as well as the nanoscopic pores of the collagen and hydrogel making up such structures.

Materials Imaging: The composite scaffolds were visually examined by confocal laser scanning microscopy, carried out on an Olympus FV1200 microscope (Olympus, JP). The materials were stained with 4′,6-diamidino-2-phenylindole (DAPI, Sigma Aldrich, UK), diluted in water by 1:1000, for 30 min. The composites were then immersed for 2 h in a 1 mg mL^{-1} solution of fluorescein isothiocyanate (FITC, Sigma Aldrich, UK) in 0.1 M NaOH, followed by washing in water overnight. DAPI was seen to bind most strongly to the collagen component, while FITC was present nonspecifically in the whole material. The resulting increased intensity of the collagen component was used to discern it from the cryogel component. The materials were imaged at a magnification of 10× using a UV laser (405 nm excitation, GaN) and a visible laser (488 nm excitation, argon ion).

Mechanical Testing: Spherical indentation was used to characterize the time-dependent mechanical response of the composite scaffolds in the neutral and activated states, as well as one of the single components subjected to the same activation steps. Testing was performed in displacement-control on a 5544 Instron universal testing machine (Instron, US) with a stainless steel tip of 4 mm diameter attached to a 5 N load cell. A ramp-hold test profile was used with a ramp of 10 s to an indentation depth of 0.1 mm, followed by a hold of 120 s, over which the load relaxation approached a plateau. The load profile with time was analyzed within viscoelastic and poroelastic frameworks, applied using algorithms based on exponential fitting of the load relaxation profile.[45,46] In particular, the viscoelastic framework was applied to the whole relaxation profile to extract the viscoelastic ratio R; the poroelastic ratio was fit to the last 10% of the profile where fluid flow has been observed to dominate relaxation,[45] and used to extract the elastic modulus E and hydraulic permeability K of the materials.

Cell Seeding Efficiency and Metabolic Activity: SW1353 chondrosarcoma cell line obtained from LGC Standards, UK, was used for all biological studies. The cells were cultured in DMEM/F-12 (Dulbecco's Modified Eagle Medium/Nutrient Mixture F-12), supplemented with fetal bovine serum (10% v/v) and penicillin–streptomycin (10 000 units mL^{-1} penicillin, 10 mg mL^{-1}streptomycin) to obtain complete medium. All reagents and kits used for cell culture were obtained from Life Technologies Ltd, UK, unless otherwise indicated. Cells were cultured in humidified atmosphere, 5% CO_2 in air at 37 °C, and the culture medium was exchanged every other day. When cells reached ≈85% confluence, they were trypsinized with 0.25% trypsin containing ethylenediamine tetraacetic acid (1 mM, EDTA) and used for the experiments. A cell suspension (1.5×10^5 cells in 50 µL) was seeded at the bottom of a 96-well plate, followed by the addition of the scaffolds on top of the cell layer and incubation for 3 h. Subsequently, the scaffolds were transferred to a new well plate, complete medium was added, and tissue culture started. At the same time, PrestoBlue dye was used to quantify the number of cells left in the plates, based on a standard curve. These were incubated for 120 min at 37 °C in a 1:10 volume of PrestoBlue reagent in complete medium. Absorbance was then measured at 570 nm (excitation) and 600 nm (emission) using a FLUOstar Optima (BMG Labtech, Germany) microplate reader. The normalized signal was obtained as the ratio of sample absorbance to the mean of control absorbance. The number of cells left in the plates was quantified by comparison with a standard curve ran for the specific purpose. SW1353 cells were cultured on the scaffolds for a period of 14 days. PrestoBlue was used to assess cellular metabolic activity throughout the study, following manufacturer guidelines. At each time point (1, 3, 5, 9, 11, and 14 days), a 1: 10 volume of PrestoBlue reagent in complete medium was added directly to each sample prior to incubation for 60 min at 37 °C. The measured signal was normalized over that recorded at day 1 to calculate the normalized metabolic activity.

Fabrication of 2D Films and Cell Culture: Films of PVA–PAA blends were fabricated by casting the 3:1 solution used for the 3D materials onto silicon molds. The cast films were dried in air, followed by heat treatment at 90 °C for 5 and 12.2 h in order to achieve a polymer volume fraction in the range of those found in the 2FT and 8FT cryogels, respectively.[11] Activation and sterilization of the PVA–PAA films were performed using the same protocol as for the 3D scaffolds. Collagen films were prepared by drying the 1% w/v suspension directly onto glass cover slips for 48 h in a laminar flow cabinet. The films were EDC/NHS-cross-linked relative to the molarity of collagen carboxylic acid groups as for 3D collagen scaffolds. Cells were seeded onto the films at 1.0×10^4 cells cm^{-2} and cultured for 14 days.

Cell Number: Cell number for the 3D and 2D materials was assessed by quantifying the DNA content of the cells cultured on the materials using the Quanti-iTTM PicoGreen dsDNA assay kit. Papain digestive solution was added to each sample and incubated overnight at 65 °C. Samples were freeze-thawed to ensure the complete lysis of the cells. A volume of 100 µL of the lysates and 100 µL of the PicoGreen solution (prepared according to the manufacturer's protocol) were added in each well of a 96-well plate. Fluorescence was measured at 485 nm excitation and 520 nm emission using a FLUOstar OPTIMA microplate reader. A standard curve of DNA was produced using known concentrations of lambda DNA (Invitrogen).

Cell Imaging: Cell depth within the 3D scaffolds was assessed using fluorescent trackers: Vybrant CFDA SE Cell Tracker Kit was used to fluorescently stain SW1353 according to the manufacturer's instruction. Cells were visualized at each time point by confocal laser scanning microscopy, utilizing the same microscope as described above. Micrographs were taken at 10× magnification using a visible laser (488 nm excitation, argon ion). Vertical stacks through the samples were acquired over 150 µm with an interval of 10 µm. The images were then projected along the z-axis using the ImageJ distribution FIJI Z-Project function. Position along the y-axis was measured using the Analyze Particles function in FIJI, and subtracted from the y-coordinate corresponding to the surface of the sample to obtain the migration distance.

Cells seeded on top of the 2D materials were stained with DAPI (nucleus) and phalloidin (cytoskeleton, Invitrogen, UK) and imaged using fluorescence microscopy (Zeiss Axiovert S100, Carl Zeiss, UK) up to day 5, after which the cells reached confluency on the collagen. Analysis of the morphology was carried out in ImageJ, FIJI distribution, using the "analyze particle" function to measure the roundness of the cells.

Statistical Analysis and Data Representation: All swelling and mechanical measurements were made on four different samples per condition. A total of ten indents were performed per condition. Biological studies on the 3D composites and single components were performed on six samples per condition/time-point. Every sample was used to measure the cell seeding efficiency on day 0 and metabolic

activity on subsequent days, after which the most representative sample between the six, that is, the one closer to the average metabolic activity, was used to image cell migration. The other five samples were used to test cell number. Each value other than migration distance is reported as mean and standard deviation of these measurements. The entire distribution measured for the migration distance is reported, together with the mean, standard deviation, and first and third quartile. For the 2D study, cell morphology was assessed for at least 14 different areas per condition, four samples per condition. The reported trends were tested for statistical significance using one-way analysis of variance (ANOVA). Where comparison between two different datasets was made, statistical significance was assessed using a paired *t*-test. All statistical analysis was performed using the software package OriginPro 2016. A probability value of 95% ($p < 0.05$) was used to determine significance for both types of tests.

Supporting Information

Supporting Information is available from the Wiley Online Library or from the author.

Acknowledgements

This work was supported by the European Research Council (ERC Advanced Grant 320598 3D-E), and the Engineering and Physical Sciences Research Council (grant EPSRC EP/G037221/1).

Conflict of Interest

The authors declare no conflict of interest.

Keywords

biomimetic cell microenvironments, collagen, composite materials, mechanical properties, polyelectrolytes

Received: July 2, 2018
Published online: September 6, 2018

[1] E. A. Makris, A. H. Gomoll, K. N. Malizos, J. C. Hu, K. A. Athanasiou, *Nat. Rev. Rheumatol.* **2015**, *11*, 21.
[2] K. M. Heinemeier, P. Schjerling, J. Heinemeier, M. B. Moller, M. R. Krogsgaard, T. Grum-Schwensen, M. M. Petersen, M. Kjaer, *Sci. Transl. Med.* **2016**, *8*, 346ra90.
[3] D. J. Huey, J. C. Hu, K. A. Athanasiou, *Science* **2012**, *338*, 917.
[4] A. R. Armiento, M. J. Stoddart, M. Alini, D. Eglin, *Acta Biomater.* **2018**, *65*, 1.
[5] A. J. Engler, S. Sen, H. L. Sweeney, D. E. Discher, *Cell* **2006**, *126*, 677.
[6] C. M. Murphy, A. Matsiko, M. G. Haugh, J. P. Gleeson, F. J. O'Brien, *J. Mech. Behav. Biomed. Mater.* **2012**, *11*, 53.
[7] R. Olivares-Navarrete, E. M. Lee, K. Smith, S. L. Hyzy, M. Doroudi, J. K. Williams, K. Gall, B. D. Boyan, Z. Schwartz, *PLoS One* **2017**, *12*, e0170312.
[8] O. Chaudhuri, L. Gu, D. Klumpers, M. Darnell, S. A. Bencherif, J. C. Weaver, N. Huebsch, H. P. Lee, E. Lippens, G. N. Duda, D. J. Mooney, *Nature Mater.* **2015**, *15*, 326.
[9] H. Lee, L. Gu, D. J. Mooney, M. E. Levenston, O. Chaudhuri, *Nature Mater.* **2017**, *16*, 1243.
[10] E. Tzima, M. Irani-Tehrani, W. B. Kiosses, E. Dejana, D. A. Schultz, B. Engelhardt, G. Cao, H. DeLisser, M. A. Schwarts, *Nature* **2005**, *437*, 426.
[11] G. S. Offeddu, I. Mela, P. Jeggle, R. M. Henderson, S. K. Smoukov, M. L. Oyen, *Sci. Rep.* **2017**, *7*, 42948.
[12] M. S. Bergholt, J. P. St-Pierre, G. S. Offeddu, P. A. Parmar, M. B. Albro, J. L. Puetzer, M. L. Oyen, M. M. Stevens, *ACS Central Sci.* **2016**, *2*, 885.
[13] V. C. Mow, A. Ratcliffe, R. Poole, *Biomaterials* **1992**, *13*, 67.
[14] F. G. Donnan, *Chem. Rev.* **1924**, *1*, 73.
[15] G. S. Offeddu, M. L. Oyen, *Smart Materials for Tissue Engineering: Fundamental Principles*, RSC publishing, Cambridge **2016**.
[16] H. J. Kwon, *Adv. Mater. Sci. Eng.* **2014**, 154071.
[17] C. M. Hassan, N. A. Peppas, *Biopolymers PVA Hydrogels, Anionic Polymerization Nanocomposites*, Springer, Medford **2000**.
[18] I. V. Yannas, J. F. Burke, D. P. Orgill, E. M. Skrabut, *Science* **1982**, *215*, 174.
[19] U. Cheema, M. Ananta, V. Mudera, *Regenerative Medicine and Tissue Engineering – Cells and Biomaterials*, InTech, Rijeka, Croatia **2011**.
[20] S. J. Kew, J. H. Gwynne, D. Enea, R. Brookes, N. Rushton, S. M. Best, R. E. Cameron, *Acta Biomater.* **2012**, *8*, 3723.
[21] J. C. Ashworth, M. Mehr, P. G. Buxton, S. M. Best, R. E. Cameron, *Adv. Healthcare Mater.* **2015**, *4*, 1317.
[22] J. J. Campbell, A. Husmann, R. D. Hume, C. J. Watson, R. E. Cameron, *Biomaterials* **2017**, *114*, 34.
[23] F. Jianqi, G. Lixia, *Eur. Polym. J.* **2002**, *38*, 1653.
[24] G. S. Offeddu, J. C. Ashworth, R. E. Cameron, M. L. Oyen, *Acta Biomater.* **2016**, *41*, 193.
[25] W. Wilson, C. C. van Donkelaar, B. van Rietbergen, R. A. Huiskes, *J. Biomech.* **2005**, *38*, 1195.
[26] X. L. Lu, L. Q. Wan, X. E. Guo, V. C. Mow, *J. Biomech.* **2010**, *43*, 673.
[27] C. Chang, D. A. Lauffenburger, T. I. Morales, *Osteoarthr. Cartil.* **2003**, *11*, 603.
[28] O. Okay, S. Durmaz, *Polymer* **2002**, *43*, 1215.
[29] F. Horkay, I. Tasaki, P. J. Basser, *Biomacromol.* **2000**, *1*, 84.
[30] L. J. Gibson, M. F. Ashby, *Cellular Solids: Structure and Properties*, Cambridge University Press, Cambridge **1999**.
[31] J. G. Williams, C. Gamonpilas, *Int. J. Solids and Structures* **2008**, *45*, 4448.
[32] F. J. O'Brien, B. A. Harley, M. A. Waller, I. V. Yannas, L. J. Gibson, P. J. Prendergast, *Technol. Health Care* **2007**, *15*, 3.
[33] F. Boschetti, C. Miotti, F. Massi, M. Colombo, V. Quaglini, G. M. Peretti, R. Pietrabissa, *Proc. Second Jt. EMBS/BMES Conf.* **2002**, 2581.
[34] A. Maroudas, *Biophys. J.* **1968**, *8*, 575.
[35] M. L. Oyen, T. A. V. Shean, D. G. T. Strange, M. Galli, *J. Mater. Res.* **2011**, *27*, 245.
[36] J. Mattice, M. L. Oyen, R. Kent, *J. Mater. Res.* **2006**, *21*, 2003.
[37] D. V. Bax, N. Davidenko, D. Gullberg, S. W. Hamaia, R. W. Farndale, S. M. Best, R. E. Cameron, *Acta Biomater.* **2017**, *49*, 218.
[38] C. Huang, K. Hu, Z. Wei, *Sci. Rep.* **2016**, *6*, 37960.
[39] M. Rabineau, F. Flick, E. Mathieu, A. Tu, B. Senger, J. C. Voegel, P. Lavalle, P. Schaaf, J. N. Freund, Y. Haikei, D. Vautier, *Biomaterials* **2015**, *37*, 144.
[40] J. P. Urban, *Biochem. Soc. Trans.* **2002**, *30*, 858.
[41] M. B. Pabbruwe, E. Esfandiari, W. Kafienah, J. F. Tarlton, A. P. Hollander, *Biomaterials* **2009**, *30*, 4277.
[42] G. F. Weber, *Front. Oncol.* **2016**, *6*, 257.
[43] P. Friedl, K. Wolf, *J. Cell Biol.* **2010**, *188*, 11.
[44] J. D. Humphreys, E. R. Dufresne, M. A. Schwarts, *Nature Rev. Mol. Cell Biol.* **2014**, *15*, 802.
[45] M. L. Oyen, *Philos. Mag.* **2006**, *86*, 5625.
[46] M. Galli, K. S. C. Comley, T. Shean, M. L. Oyen, *J. Mater. Res.* **2009**, *24*, 973.